Nanoscale

PAPER

Cite this: *Nanoscale*, 2018, **10**, 15793

A CuO-functionalized NMOF probe with a tunable excitation wavelength for selective detection and imaging of H_2S in living cells†

Yu Ma, Caiyun Zhang, Peng Yang, Xiangyuan Li, Lili Tong, Fang Huang, Jieyu Yue and Bo Tang *

Received 5th May 2018,
Accepted 18th July 2018

DOI: 10.1039/c8nr03651a

rsc.li/nanoscale

Recently, fluorescent nanoscale metal–organic frameworks (NMOFs) have been proven to be useful probes for the detection and imaging of active biomolecules in living cells. However, the excitation wavelengths of these NMOF fluorescence probes are mostly in the ultraviolet region, which unavoidably results in reduced cell activity, limited tissue penetration depth and inevitable biological background interference. Herein, to solve this problem, a CuO functionalized NMOF probe with a tunable excitation wavelength based on Förster resonance energy transfer (FRET) for selective detection and imaging of the third important gaseous signaling molecule hydrogen sulfide (H_2S) in living cells as an example is presented. In the energy transfer system, NMOF confines the luminophore organic dye thiazole orange within its intrinsic porous matrix as the energy donor, in which the excitation wavelength of the NMOF can be tuned simply from UV to Vis through the choice of dye molecules, and the H_2S-responding site copper oxide nanoparticle (CuO NP) is the acceptor. After the surface functionalization of CuO NPs onto the NMOF, the fluorescence of the NMOF can be efficiently quenched based on the FRET. When H_2S appeared, the fluorescence of the nanoprobe is recovered due to the interruption of FRET. This facile yet powerful strategy not only provides an instantaneous fluorescence probe for selective H_2S detection in living cells but also offers a valuable approach for using porous NMOFs to sense other biological species.

Introduction

Nanoscale metal–organic frameworks (NMOFs), as a new type of miniature crystalline porous MOF material, self-assembled from metal ions/clusters and organic bridging ligands, have attracted great attention in chemical sensing and biological applications.[1–4] Compared with the bulk crystals of MOF materials, these NMOFs exhibited some unique advantages in their applications.[5] There into, luminescent NMOFs have been widely used as fluorescence probes for selectively detecting and imaging a range of active biological species, due to their high specific surface areas and porosity, easier functionalization, structural diversity and good biodegradability.[1–4] However, the excitation wavelengths of these NMOF fluorescence probes are mostly in the ultraviolet region, which unavoidably results in reduced cell activity, limited tissue penetration depth and inevitable biological background interference. The main reason for the problem is that the variations of fluorescence intensities in response to the analyte for most NMOF probes mainly originate from the fluorescence organic ligands. And the absorption wavelengths for most of the organic bridging ligands being used currently are in the ultraviolet region except for only a few porphyrin derivative ligands, which have been used in photodynamic therapy for the reactive oxygen species production to kill tumor cells.[6–11] Considering that some drawbacks are unavoidable for constructing visible or infrared organic fluorescence ligands modified from specific fluorophores, such as multistep synthesis and difficult separation, we believe that a convenient construction strategy for a novel NMOF probe with a tunable excitation wavelength based on a simply confined luminophore organic dye within the intrinsic porous matrix of the NMOF is an alternative promising method to tune the excitation wavelength of NMOF materials.

For a proof-of-concept demonstration, we select hydrogen sulfide (H_2S), which has been regarded as one of the most important gaseous signaling molecules in living

College of Chemistry, Chemical Engineering and Materials Science, Key Laboratory of Molecular and Nano Probes, Ministry of Education, Collaborative Innovation Center of Functionalized Probes for Chemical Imaging in Universities of Shandong, Institute of Molecular and Nano Science, Shandong Normal University, Jinan 250014, P. R. China. E-mail: tangb@sdnu.edu.cn; Fax: +(86)53186180017

†Electronic supplementary information (ESI) available: PXRD patterns, EDS images, fluorescence spectra, UV-vis absorption spectra and MTT assay. See DOI: 10.1039/c8nr03651a

organisms,[12–15] as the object for selective detection and imaging. This endogenous gaseous signaling molecule has been demonstrated to be related to numerous physiological processes, for example immune response, angiogenesis, antioxidation, neurotransmission and apoptosis.[16–20] However, abnormal expression of this signaling molecule has also been related to many pathological processes, such as Parkinson's, diabetes, Alzheimer's disease, Down syndrome, liver cirrhosis and even cancer.[21–26] Consequently, the detection of these biomolecules, mainly biosynthesized by enzymatic reactions in the mitochondria or cytosol in living cells,[27] is of great importance. Although very recently fluorescent NMOFs have also been proven to be useful probes for H_2S detection in living cells, the common optical excitation problem for these H_2S NMOF probes also exists.[28–35]

Herein, to solve the problem originating from the ultraviolet excitation, we present a simple yet useful surface functionalized NMOF probe based on FRET for endogenous H_2S detection. Typically, the H_2S fluorescence probe consists of NMOFs that confine dyes in the pores, the surface functionalization material hexadecyl trimethyl ammonium bromide (CTAB) and copper oxide nanoparticles (CuO NPs). Considering the excellent adsorption properties of the NMOF material based on its porous matrix, the luminophore organic dye thiazole orange was firstly confined in the pores of a Zr-UiO-66 MOF (TO@UiO-66) to adjust the absorption wavelength of the NMOF and simultaneously minimize the aggregation-caused fluorescence quenching of the fluorophore.[36,37] As the surface functionalization material could improve the stability of NMOFs and the interaction between nanoparticles, the cationic surface functionalization material CTAB was then added to functionalize the NMOF surface and combine with CuO NPs conveniently through multiple weak interactions (electrostatic interaction, hydrogen bond interaction, *etc*.) based on the abundant electron-rich hydroxyl and carboxyl groups on the surface of CuO NPs and NMOFs.[38] After the surface functionalization of CuO NPs onto the NMOFs, Förster resonance energy transfer (FRET) was realized by TO@UiO-66 as the donor and CuO NPs as the acceptor. As the H_2S-responding site, the CuO NPs can efficiently quench the fluorescence of the NMOF *via* FRET. While the CuO NPs react with H_2S at physiological pH to produce copper sulfide, the FRET between the donor and acceptor can be interrupted and the fluorescence based on TO@UiO-66 was, thus, obtained simultaneously. The design strategy for the H_2S nanoprobe is shown in Fig. 1.

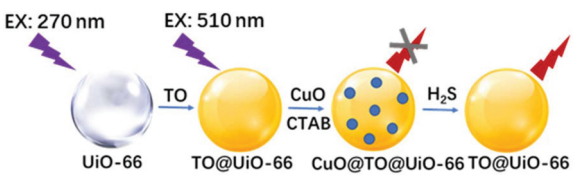

Fig. 1 Schematic representation of the design strategy for the H_2S nanoprobe based on NMOFs.

Experimental

Materials and methods

Materials. Terephthalic acid (H_2BDC), zirconyl chloride octahydrate, glacial acetic acid, thiazole orange, cupric acetate monohydrate, hexadecyl trimethyl ammonium bromide, sodium hydrosulfide, NaClO, Na_2SO_3, Na_2SO_4, KSCN, $Na_2S_2O_3$, Na_2HPO_4, Na_2CO_3, NaH_2PO_4, $NaHSO_3$, $NaNO_2$, NaCl, $NaHCO_3$, homocysteine (Hcy), cysteine (Cys), glutathione (GSH), hydrogen peroxide (H_2O_2), *S*-nitroso-*N*-acetyl-DL-penicillamine (SNP) and Dulbecco's modified Eagle's medium (DMEM) were obtained from Sigma-Aldrich (Shanghai, China). All these chemicals that were obtained from commercial sources were used without further purification. The human hepatocellular liver carcinoma cell line HepG2 and human lung carcinoma cell line A549 were both purchased from the Committee on Type Culture Collection of the Chinese Academy of Sciences.

Physical measurements. A Bruker SMART APEX CCD-based diffractometer has been used to obtain Powder X-ray Diffraction (PXRD) patterns. A scanning electron microscope (SUPRA 55) has been used to perform Energy dispersive spectroscopy (EDS) mapping analysis. A JEM-100CX II electron microscope has been employed to record transmission electron microscopy (TEM) images. The fluorescence spectra were obtained on a FLS-920 Edinburgh fluorescence spectrometer. Absorption spectra were obtained by using a TU-1900 UV-vis spectrophotometer. The time-dependent fluorescence spectra were recorded on a Cary Eclipse spectrofluorometer (Varian, Australia). The fluorescence images were obtained by using a Leica TCS SP8 with 488 nm excitation. In the MTT assay, absorbance was recorded on a microplate reader (Synergy 2, Biotek, USA).

Synthesis of TO@UiO-66. Firstly, UiO-66 was synthesized according to the literature with minor modification.[39] A dimethylformamide solution of CH_3COOH (0.3 mL), $ZrOCl_2{\cdot}8H_2O$ (65 μmol, 0.021 g) and H_2BDC (0.3 mmol, 0.050 g) was sonicated for 15 min at room temperature. Then, the solution was transferred into a 23 mL Teflon-lined autoclave and heated at 90 °C for 20 h. After cooling to room temperature, nanoscale crystals were collected, washed with dimethylformamide and ethanol, and then dried in a vacuum. After the phase purity of the nanoscale crystals was verified by PXRD, 0.020 g UiO-66 was added to a thiazole orange aqueous solution (5 mL, 1 mg mL^{-1}) and stirred for 3 days at room temperature. Finally, the nanoscale crystals were collected and washed with water several times.

Synthesis of CuO NPs. CuO NPs were synthesized according to the literature with minor modification.[40] $Cu(CH_3COO)_2{\cdot}H_2O$ (0.25 mmol, 0.050 g) was first dissolved in ethanol in a 23 mL Teflon-lined autoclave and heated at 110 °C for 20 h. After cooling to room temperature, the nanoparticles were obtained by centrifugal separation and washed with water and ethanol.

Synthesis of CuO@TO@UiO-66. TO@UiO-66 was dispersed in water (0.2 mg mL^{-1}) and then 0.050 g CTAB was added. After stirring for two hours, an aqueous solution of pre-synthesized CuO NPs was added drop by drop. After being stirred

for another 2 hours, the final product was collected by centrifugal separation and washed with water three times.

Confocal imaging. HepG2 cells were firstly incubated for 24 h in confocal dishes. The nanoprobe (10 μg mL^{-1}) was then transferred into these cells in DMEM medium containing 10% FBS. These cells were further incubated for another 4 h and washed with Tris-HCl buffer. Then, after the cells were incubated with 50 μM NaHS for another 30 min, confocal images with 488 nm excitation were immediately recorded by using a CLSM with a He–Ne laser, and the emission was collected between 520 and 650 nm.

Subsequently, the imaging of A549 cells followed a similar procedure that for HepG2 cells, except that the RPMI medium 1640 was substituted for the DMEM medium, and before the nanoprobe (10 μg mL^{-1}) was delivered into the cells, A549 cells have been pretreated with SNP (500 μM) or with SNP (500 μM) and PPG (250 mg L^{-1}) for 1 h, respectively.

MTT assay. The cytotoxicity of the probe was further evaluated by using human hepatocellular liver carcinoma cells. HepG2 cells were seeded in 96-well plates (200 μL per well). After being incubated for 24 h, these HepG2 cells were cocultured with different concentrations of the nanoprobe (0.5, 1, 5, 10, 30, 50, 80 and 100 μg mL^{-1}) for another 24 h. Then, the MTT solution was delivered into all wells and then removed after 4 h. Subsequently, after the formed formazan crystals were dissolved in 150 μL DMSO, a TRITURUS microplate reader was employed to record the absorbance of the cells at 490 nm.

Results and discussion

Synthesis and characterization of the probe

The UiO-66 NMOFs were first synthesized by a solvothermal method according to the literature with minor modification[39] and the phase purity of the products was then confirmed by PXRD (Fig. S1†). TO@UiO-66 was then obtained by encapsulating luminophore organic dye thiazole orange in the pores of UiO-66. Next, the surface of the TO@UiO-66 was modified with the chemically directed surfactant assembly agent CTAB. After the preparation of CuO NPs by a hydrothermal method according to the literature, the CuO@TO@UiO-66 nanoprobe was conveniently obtained by adding an aqueous solution of the precursor CuO NPs dropwise to the solution of CTAB modified TO@UiO-66 precursor. This successful assembly of the CuO and TO@UiO-66 nanoparticles was confirmed by TEM (Fig. 2). The PXRD patterns of the composites matched well with the as-synthesized samples of the CuO NPs and the NMOF, respectively (Fig. S1†). EDS analysis further demonstrated that CuO NPs have been successfully functionalized onto the Zr/Cu hybrid nanoprobe (Fig. S2†). Additionally, we investigated the stability of the nanoprobe. Specifically, 0.1 mg composites were dispersed in aqueous solutions (Tris-HCl buffer, pH = 7.4). After a certain period of time, absorption experiments were performed with the supernatant. As shown in Fig. S3,† the absorption peak of thiazole orange and other relative components was not detected, indicating that the composite was stable under physiological conditions. And after being treated with NaHS, the probe can still maintain its good morphology (Fig. S4†).

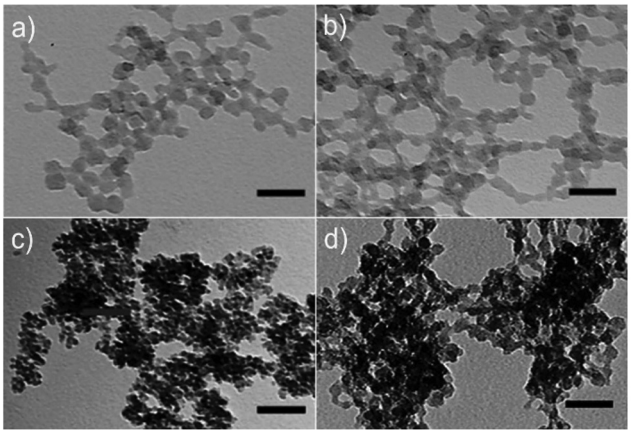

Fig. 2 TEM image of (a) UiO-66, (b) TO@UiO-66, (c) CuO NPs and (d) CuO@TO@UiO-66. Scale bar = 50 nm.

Spectroscopic properties of the NMOF probe toward H_2S

To further certify the formation of the CuO-functionalized NMOF probe, the optical properties of these precursors and the nanoprobe were evaluated. Nanocrystals of UiO-66 prepared without the luminophores exhibited only an absorption band centered at 270 nm (Fig. S5†), attributable to the BDC ligand. The TO@UiO-66 nanocrystals with the encapsulated luminophores not only showed the characteristic absorption peak of UiO-66, but also exhibited the absorption band of the organic dye thiazole orange (Fig. S5†). And the amount of thiazole orange incorporated into the UiO-66 framework was about 1.8 wt% calculated by UV-vis absorption (Fig. S6 and S7†). Additionally, from Fig. S8,† we can see that the absorption of CuO NPs is in the range from 250 to 700 nm, and this absorption band of CuO NPs overlapped with the emissions of the TO@UiO-66 composite, which provided the possibility for the generation of effective FRET between CuO NPs and the TO@UiO-66 composite. To further prove that the CuO NPs were indeed functionalized onto the surface of NMOFs, the fluorescence spectra for TO@UiO-66, a physical mixture of TO@UiO-66 and CuO nanoparticles, and CuO-functionalized TO@UiO-66 were recorded. As can be seen from Fig. S9,† while a significant decrease of the fluorescence intensity due to the FRET for the nanoprobe was observed, the change of the fluorescence intensity of the mixture was not obvious compared with free TO@NMOF. These results suggested that we have successfully functionalized CuO NPs onto the NMOFs. Then, the quenching efficiencies on the fluorescence emission of TO@UiO-66 with different amounts of CuO nanoparticles (0–200 μM) were determined. The results in Fig. S10† clearly indicated that with an enhancement of the CuO content in the nanoprobe, the fluorescence emission of this nanoprobe decreased gradually.

Subsequently, the fluorescence responses of this nanoprobe to H_2S were investigated. As shown in Fig. 3a, with the increased concentrations of H_2S ranging from 0 to 100 μM, the fluorescence intensity of the probe enhanced gradually. The reason for this fluorescence enhancement of this fluorescence probe was that the energy acceptor CuO NPs in the FRET system has reacted with H_2S at physiological pH. A good linear relationship between the H_2S concentrations and the enhanced fluorescence intensity was obtained (Fig. 3b). And the detection limit of this nanoprobe was calculated to be as low as 0.51 μM, which is comparable to that of the most sensitive NMOF probes for H_2S.[27–35,41,42] Furthermore, time-dependent fluorescence spectra of this probe showed that this probe with CuO as responding sites can detect H_2S in an instantaneous mode, which is essential for real-time detection in living cells (Fig. 3d).

The selectivity experiments were then carried out. As shown in Fig. 3c, compared with the significant fluorescence enhancement produced by the addition of 100 μM NaHS, a very limited fluorescence response was observed with abundant biologically relevant thiol and other reactive individual species, including reactive oxide species, inorganic anions, *etc*. The results indicated that the novel nanoprobe should be able to selectively detect H_2S in living cells.

Confocal imaging of the NMOF probe in living cells

Inspired by the above results, the probe was employed to detect H_2S in living cells. HepG2 cells with or without this nanoprobe were first prepared. As depicted in Fig. 4a, when HepG2 cells were incubated with 10 μg mL^{-1} nanoprobe, only negligibly weak fluorescence was observed. Fig. 4b shows the corresponding bright-field image. Upon addition of NaHS (50 μM), an obvious enhancement of fluorescence intensity was observed in Fig. 4c, demonstrating that this nanoprobe was able to detect H_2S in living cells. Simultaneously, the bright-field images proved the good biocompatibility of this probe. Additionally, an MTT assay based on HepG2 cells also demonstrated that this nanoprobe has good biocompatibility (Fig. S11†).

Next, to estimate the capability of the nanoprobe for endogenous H_2S detection, we further detected and imaged H_2S in human A549 cells. It has been demonstrated that H_2S can regulate the redox signaling of A549 cells and the high contents of cystathionine γ-lyase (CSE) and cystathionine β-synthase (CBS) enzymes are essential for the production of H_2S.[43] Then, we employed SNP (a NO donor) to upregulate the activity of CSE and CBS[44] and thus to induce the production of H_2S in human A549 cells. As can be seen from Fig. 4e, after the nanoprobe was coincubated with SNP treated A549 cells, a strong fluorescence from the nanoprobe (10 μg mL^{-1}) appeared. Differently, when DL-propargylglycine (PPG, an inhibitor of CSE and CBS)[22] was transferred into the cells before these cells were coincubated with SNP, the fluorescence from the nanoprobe was negligible (Fig. 4g). All these results demonstrated that this nanoprobe is indeed able to detect endogenous H_2S in living cells.

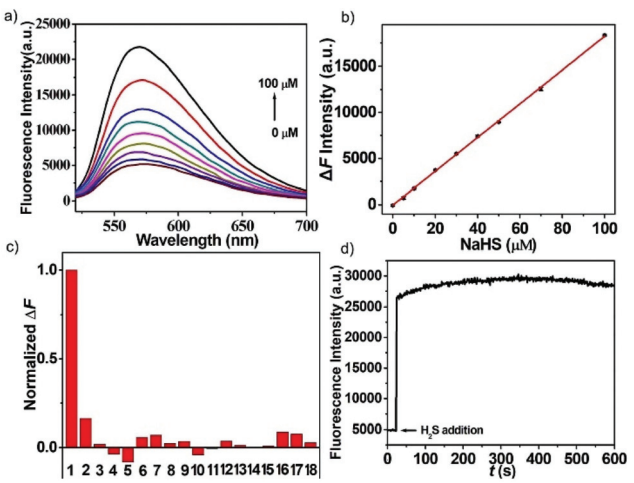

Fig. 3 (a) Fluorescence spectra of the nanoprobe (0.1 mg mL^{-1}) in Tris-HCl butter (pH = 7.40) obtained upon titration with NaHS from 0 to 100 μM, λ_{ex} = 510 nm; (b) linear relationship between the concentration of NaHS and the enhanced fluorescence intensity (Δ*F*); (c) fluorescence variation of the nanoprobe to different reactive species: (1) HS^- (100 μM), (2) GSH (10 mM), (3) ClO^- (200 μM), (4) NO (200 μM), (5) H_2O_2 (200 μM), (6) SO_3^{2-} (1 mM), (7) HCO_3^- (1 mM), (8) SCN^- (1 mM), (9) SO_4^{2-} (1 mM), (10) $S_2O_3^{2-}$ (1 mM), (11) HPO_4^{2-} (1 mM), (12) $H_2PO_4^-$ (1 mM), (13) HSO_3^- (1 mM), (14) NO_2^- (1 mM), (15) CO_3^{2-} (1 mM), (16) L-Cys (100 μM), (17) Hcy (100 μM) and (18) Cl^- (1 mM), respectively; (d) time-dependent fluorescence spectra of the nanoprobe with addition of 100 μM NaHS in Tris-HCl buffer (20 mM, pH = 7.4).

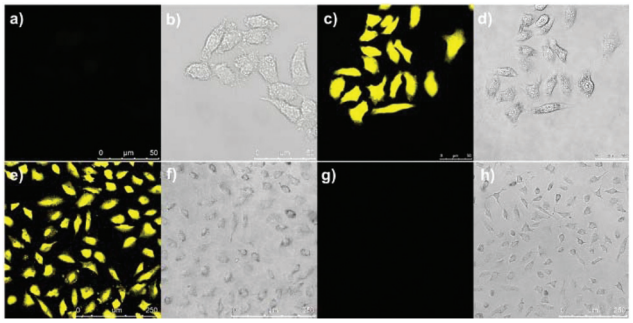

Fig. 4 Confocal fluorescence images: (a) and (b) HepG2 cells with only the nanoprobe (10 μg mL^{-1}); (c) and (d) HepG2 cells with the nanoprobe (10 μg mL^{-1}) and NaHS (50 μM); (e) and (f) A549 cells with the nanoprobe (10 μg mL^{-1}) and SNP (500 μM); (g) and (h) A549 cells with the nanoprobe (10 μg mL^{-1}), PPG (250 mg L^{-1}) and SNP (500 μM).

Conclusions

To solve the problem that the NMOF fluorescence probe with ultraviolet excitation unavoidably results in reduced cell activity, limited tissue penetration depth and inevitable biological background interference, we present a simple yet useful CuO functionalized NMOF probe with a tunable excitation wavelength based on FRET for selective detection and imaging of endogenous H_2S in living cells. In this energy transfer

system, the NMOF confined luminophore organic dye TO within its intrinsic porous matrix is the energy donor, in which the excitation wavelength of the NMOF can be tuned simply from UV to Vis through the choice of dye molecules, and the H_2S-responding site CuO NP is the acceptor. After the nanoprobe was delivered into HepG2 and A549 cells, the fluorescence of the probe based on TO with 488 nm excitation is recovered due to the interruption of FRET. This facile yet powerful construction strategy for the FRET-based fluorescence probe, assembled from the NMOF encapsulated selected organic dye within its intrinsic porous matrix and the responding site with a quenching effect, not only provided an instantaneous fluorescence nanoprobe for selective H_2S detection in living cells but also offer a valuable approach for using porous NMOFs to sense other biological species with a tunable excitation wavelength.

Conflicts of interest

There are no conflicts to declare.

Acknowledgements

This work was supported by National Natural Science Foundation of China (21535004, 91753111, 21675103, 21602126, 21390411) and Key Research and Development Program of Shandong Province (2018YFJH0502).

Notes and references

1 M. Giménez-Marqués, T. Hidalgo, C. Serre and P. Horcajada, *Coord. Chem. Rev.*, 2016, **307**, 342–360.
2 F. Y. Yi, D. Chen, M. K. Wu, L. Han and H. L. Jiang, *ChemPlusChem*, 2016, **81**, 675–690.
3 L. E. Kreno, K. Leong, O. K. Farha, M. Allendorf, R. P. Van Duyne and J. T. Hupp, *Chem. Rev.*, 2012, **112**, 1105–1125.
4 Z. Hu, B. J. Deibert and J. Li, *Chem. Soc. Rev.*, 2014, **43**, 5815–5840.
5 A. Carne, C. Carbonell, I. Imaz and D. Maspoch, *Chem. Soc. Rev.*, 2011, **40**, 291–305.
6 Y. Ma, X. Li, A. Li, P. Yang, C. Zhang and B. Tang, *Angew. Chem.*, 2017, **129**, 13940–13944, (*Angew. Chem. Int. Ed.*, 2017, **56**, 13752–13756).
7 J. Park, Q. Jiang, D. Feng, L. Mao and H. C. Zhou, *J. Am. Chem. Soc.*, 2016, **138**, 3518–3525.
8 J. Park, Q. Jiang, D. W. Feng and H.-C. Zhou, *Angew. Chem.*, 2016, **128**, 7304–7309, (*Angew. Chem. Int. Ed.*, 2016, **55**, 7188–7193).
9 K. D. Lu, C. B. He and W. B. Lin, *J. Am. Chem. Soc.*, 2014, **136**, 16712–16715.
10 K. D. Lu, C. B. He and W. B. Lin, *J. Am. Chem. Soc.*, 2015, **137**, 7600–7603.
11 K. D. Lu, C. B. He, N. N. Guo, C. Chan, K. Y. Ni, R. R. Weichselbaum and W. B. Lin, *J. Am. Chem. Soc.*, 2016, **138**, 12502–12510.
12 T. S. Bailey and M. D. Pluth, *J. Am. Chem. Soc.*, 2013, **135**, 16697–16704.
13 L. Li, P. Rose and P. K. Moore, *Annu. Rev. Pharmacol. Toxicol.*, 2011, **51**, 169–187.
14 R. Wang, *FASEB J.*, 2002, **16**, 1792–1798.
15 E. Culotta and D. E. Koshland, *Science*, 1992, **258**, 1862–1865.
16 V. S. Lin, A. R. Lippert and C. J. Chang, *Proc. Natl. Acad. Sci. U. S. A.*, 2013, **110**, 7131–7135.
17 A. Papapetropoulos, A. Pyriochou, Z. Altaany, G. Yang, A. Marazioti, Z. Zhou, M. G. Jeschke, L. K. Branski, D. N. Herndon, R. Wang and C. Szabó, *Proc. Natl. Acad. Sci. U. S. A.*, 2009, **106**, 21972–21977.
18 J. W. Calvert, S. Jha, S. Gundewar, J. W. Elrod, A. Ramachandran, C. B. Pattillo, C. G. Kevil and D. J. Lefer, *Circ. Res.*, 2009, **105**, 365–374.
19 K. Abe and H. J. Kimura, *J. Neurosci.*, 1996, **16**, 1066–1071.
20 G. D. Yang, L. Y. Wu and R. Wang, *FASEB J.*, 2006, **20**, 553–555.
21 B. D. Paula and S. H. Snyder, *Biochem. Pharmacol.*, 2018, **149**, 101–108.
22 W. M. Zhao, J. Zhang, Y. J. Lu and R. Wang, *EMBO J.*, 2001, **20**, 6008–6016.
23 P. K. Kamat, P. Kyles, A. Kalani and N. Tyagi, *Mol. Neurobiol.*, 2015, **53**, 2451–2467.
24 P. Kamoun, M. C. Belardinelli, A. Chabli, K. Lallouchi and B. Chadefaux-Vekemans, *Am. J. Med. Genet., Part A*, 2003, **116**, 310–311.
25 S. Fiorucci, E. Antonelli, A. Mencarelli, S. Orlandi, B. Renga, G. Rizzo, E. Distrutti, V. Shah and A. Morelli, *Hepatology*, 2005, **42**, 539–548.
26 C. Szabo, C. Coletta, C. Chao, K. Modis, B. Szczesny, A. Papapetropoulos and M. R. Hellmich, *Proc. Natl. Acad. Sci. U. S. A.*, 2013, **110**, 12474–12479.
27 D. Boehning and S. H. Snyder, *Annu. Rev. Neurosci.*, 2003, **26**, 105–131.
28 X. Zhang, Q. Hu, T. Xia, J. Zhang, Y. Yang, Y. Cui, B. Chen and G. Qian, *ACS Appl. Mater. Interfaces*, 2016, **8**, 32259–32265.
29 Y. Y. Cao, X. F. Guo and H. Wang, *Sens. Actuators, B*, 2017, **243**, 8–13.
30 A. Buragohain and S. Biswas, *CrystEngComm*, 2016, **18**, 4374–4381.
31 H. Li, X. Feng, Y. Guo, D. Chen, R. Li, X. Ren, X. Jiang, Y. Dong and B. Wang, *Sci. Rep.*, 2014, **4**, 4366–4370.
32 S. S. Nagarkar, T. Saha, A. V. Desai, P. Talukdar and S. K. Ghosh, *Sci. Rep.*, 2014, **4**, 7053–7058.
33 Y. Ma, H. Su, X. Kuang, X. Li, T. Zhang and B. Tang, *Anal. Chem.*, 2014, **86**, 11459–11463.
34 A. Das, S. Banesh, V. Trivedib and S. Biswas, *Dalton Trans.*, 2018, **47**, 2690–2700.
35 X. L. Xin, J. X. Wang, C. F. Gong, H. Xu, R. M. Wang, S. J. Ji, H. X. Dong, Q. G. Meng, L. L. Zhang, F. N. Dai and D. F. Sun, *Sci. Rep.*, 2016, **6**, 21951.

36 M. Handke, T. Adachi, C. H. Hu and M. D. Ward, *Angew. Chem., Int. Ed.*, 2017, **56**, 14003–14006.
37 J. C. Yu, Y. J. Cui, H. Xu, Y. Yang, Z. Y. Wang, B. L. Chen and G. D. Qian, *Nat. Commun.*, 2013, **4**, 2719.
38 D. T. Lee, J. Zhao, G. W. Peterson and G. N. Parsons, *Chem. Mater.*, 2017, **29**, 4894–4903.
39 J. H. Cavka, S. R. Jakobsen, U. Olsbye, N. Guillou, C. Lamberti, S. Bordiga and K. P. Lillerud, *J. Am. Chem. Soc.*, 2008, **130**, 13850–13851.
40 Z. S. Hong, Y. Cao and J. F. Deng, *Mater. Lett.*, 2002, **52**, 34–38.
41 Q. Gao, S. Y. Xu, C. Guo, Y. G. Chen and L. Y. Wang, *ACS Appl. Mater. Interfaces*, 2018, **10**, 16059–16065.
42 X. L. Xin, F. N. Dai, F. G. Li, X. Jin, R. M. Wang and D. F. Sun, *Anal. Methods*, 2017, **9**, 3094–3098.
43 M. Nishida, T. Sawa, N. Kitajima, K. Ono, H. Inoue, H. Ihara, H. Motohashi, M. Yamamoto, M. Suematsu, H. Kurose, A. van der Vliet, B. A. Freeman, T. Shibata, K. Uchida, Y. Kumagai and T. Akaike, *Nat. Chem. Biol.*, 2012, **8**, 714–724.
44 B. D. Paul and S. H. Snyder, *Nat. Rev. Mol. Cell Biol.*, 2012, **13**, 499–507.